Numerical Study of the Entrance Flow and Its Transition in a Circular Pipe (2)

By

H. KANDA and K. OSHIMA

(February 5, 1987)

Summary: The experimental data and results of prior investigations lead to defining the problem of the transition from laminar to turbulent flow in a circular pipe. So far, the subject has been a major problem for hydro- and aeromechanics, and yet it seems not to have been clearly defined. Therefore, the flow field of a circular pipe is examined with particular emphasis on the entrance and transition length, using the two-dimentional computational scheme presented at the Symposium on Mechanics for Space Flight-1985 at ISAS. Symmetric disturbances were superimposed on points near the inlet and wall of the pipe. It was, for the first time, found that the transition length is predicted fairly satisfactorily by the computational simulation.

1. INTRODUCTION

1.1 Classification of Research

The prediction of instability in the Hagen-Poiseuille flow is one of the most interesting, unsolved classical problems, although many researchers have studied it since Hagen (1839) and Poiseuille (1841).

There are two types of flow in a circular pipe: laminar and turbulent as seen in Fig. 1. At lower Reynolds numbers the velocity profiles are stable against most of disturbances, and a color-dye filament flows in a straight line (laminar). At higher Reynolds numbers the straight line breaks down and the color-dye filament mixes with the surrounding water (turbulent). For a laminar flow, the velocity profile grows from uniform at the inlet to a fully- developed, parabolic form at the entrance length (Fig. 2). The entrance length *zep* is usually expressed in a dimensionless form; that is, the length divided by the diameter of a pipe and the Reynolds number: $Lep=zep/(D^*Re)$ where *Lep* is the dimensionless entrance length, *D* is the diameter of a pipe and *Re* is the Reynolds number based on the pipe diameter. A subscript "*p*" means parabolic. A dimensionless axial length from the inlet is expressed in a form of $z^*=z/(DRe)$. At the entrance length, z^* is equal to *Lep*. Moreover, *Lep* is denoted as Eq. (1), which shows that *Lep* is the entrance length per flow rate.

$$L_{ep}=\frac{z_{ep}}{DRe}=\frac{z_{ep}}{\frac{UD^2}{\nu}}=\frac{z_{ep}}{\frac{4Q}{\pi\nu}} \tag{1}$$

---

* IBM Japan, Technical Education

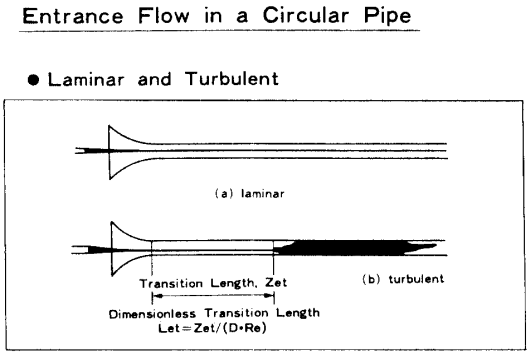

Fig. 1. Laminar and turbulent flow.

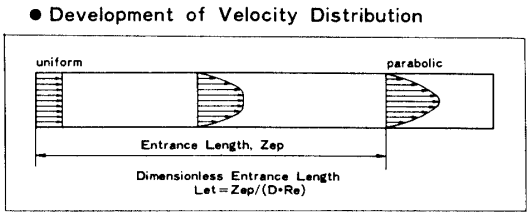

Fig. 2. Development of velocity distribution.

where, U is the average axial velocity, ν is the kinematic viscocity and Q denotes the total flux across a section: $Q=\pi UD^2/4$. It was calculated 0.1 for Reynolds numbers of above 50 [10].

So far, however, the transition length *zet*, which is the distance from the inlet to the point where the transition from laminar to turbulent flow occurs, is often presented in a dimensionless length divided only by the diameter of a pipe. In order to compare the entrance langth to the transition length, the same dimensionless unit is strongly desirable: $Let=zet/(DRe)$ where Let is the dimensionless transition length shown in Fig. 1. A subscript "t" means turbulent.

In general, investigations on the problem are categorized by four approaches: experimetnal approach, stability analysis, theoretical analysis, and direct numerical simulation (Table 1). Moreover, research efforts have been classified into two simple groups according to whether they concentrated on the entrance region or on an area farther into the pipe. In Table 1, symbols "○" and "×" indicate, respectively, whether the transition took place or not.

In short, we can easily find that most of the symbols "○" belong to the "entrance region" group of Table 1. Thus, the transition takes place very often in the entrance region. Reynolds' observations [23] have been, unfortunately, quite neglected until recently:

"Under no circumstances would be disturbance occur nearer to the trumpet than about 30 diameters in any of the pipes, and the flashes generally, but not always, commenced at about this distance."

1.2 Entrance Length

Through theoretical analysis and computational simulation, the entrance length, velocity distributions, and pressure drops are numerically calculated for the flow in the entrance region. In this region, a larger pressure drop per unit length than that in a fully developed region is required since velocities are accelerated from uniform at the inlet to a parabolic profile. Moreover, boundary layers are formed in the entrance region. Boussinesq [21] was the first to investigate theoretically the flow field in the entrance region and obtained the dimensionless entrance length of 99% of the fully developed value: $Lep=0.065$. Boussinesq's value $Lep=0.065$ seems to be in agreement with the Nikuradse's experimental data taken at some distance away from

Table 1. Research Categories

Approach	Entrance region		Fully devel. region	
Experiment				
	Arakawa, Matsunobu	○	Leite	×
	Hagen	○	Leite	○
	Kirsten	○	Stettler, Hussain	○
	Nikuradse			
	Oshima, Kanda	○		
	Poiseuille			
	Ramaprian, Tu	○		
	Reynolds	○		
	Schiller	○		
Theoretical analysis				
	Boussinesq	×		
	Langhaar	×		
	Mohanty, Asthana	×		
	Schiller	×		
	Sparrow, Lin	×		
Stability analysis				
	Huang, Chen	○	Davey, Drazin	×
	Kuwabara S.	○		
	Tatsumi	○	Garg, Rouleau	×
			Gill	×
			Salwen, Grosch	×
Numerical simulation				
	Dixon, Hellums	○	Kyrazis	×
	Kanda, Oshima	×		
	Kanda, Oshima	○		
	Kawamura	○		
	Koyari	×		
	Vrentas	×		

the inlet. Schiller [25] calculated it by assuming that velocity profiles are constant near the central core and parabolic near the wall: Lep=0.0288. The velocity profiles by Schiller show good agreement with Nicuradse's data for about a third of the initial length from the inlet [26]. Langhaar [17] obtained Lep=0.0575 for 99% of the fully developed value, by using the Bessel function. The analysis of Mohanty and Asthana [20] presented Lep=0.075 for 99.9% of the fully developed value by dividing the entrance region into two parts. Boundary-Layer approximation is applied to the first part, and therefore the value is considered reasonable above Re 500.

Recently, computers can be used to numerically simulate time dependent flow phenomena and to create detailed pictures of flow fields. By a computational numerical approach, the solution of the complete Navier-Stokes equations can be obtained for given initial and boundary conditions, although the three-dimensional solution is limited. For the problem, it is simply assumed that a uniform velocity exists at the inlet of a pipe. However, Vrentas, Duda, and Bargeron [30] assumed that the developing velocity field in the entrance region will singnificantly influence the

Table 2. Summary of Entrance Length

Authors	*Re*	*Lep*	% of fully devel. val.	Notes
Boussinesq		.65		
Langhaar,		.575	99	Bessel functions
Leite		.052		experiment, Re=13,000
Mohanty,	>500	.075	99.9	Boundary-Layer
Sciller		.02875	100	parabolic profile
Kanda, Oshima	>50	.045	98	Numerical simu.
Kanda, Oshima	>50	.055	99	Numerical simu.
Kanda, Oshima	>50	.1	100	Numerical simu.
Koyari	60	.136	98	downstream end
Koyari	60	.0325		$-dp/dr=0$
Kyrazis		.04		$v=0$
Vrentas	1	.33	99	Numerical simu.
Vrentas	50	.047	99	Numerical simu.
Vrentas	150	.048	99	Numerical simu.
Vrentas	250	.0535	99	Numerical simu.
Vrentas		.0562	99	Boundary-Layer

velocity field in the upstream region. The upstream conditions have a strong influence on the velocity field in the entrance region below a Reynolds number of 50, but no influence above a Reynolds number of 150. The entrance length for 99% of the fully-developed value is obtained by an iterative method: Lep=0.33, 0.047, 0.048, 0.0535, and 0.0562 at Reynolds numbers 1, 50, 150, 250, and under Boundary-Layer approximation, respectively. Kyrazis [16] showed that the assumption of parallel flow for the linear stability theory is invalied in the portion of the entrance region in which stability calculations have been made. The radial velocity is as high as 19% of the mean flow at z^*=0.004 and, even as far downstream as z^*=0.01, radial velocity reaches a value of 12% of the mean flow. The entrance length was arbitrarily defined as the length from the inlet to a point where the maximum radial velocity component is less than one percent of the mean flow velocity. Then the numerical results show that Lep is 0.04 at a Reynolds number of 50. Koyari [14] considered the entrance length as a distance from the inlet to a point where a radial pressure gradient vanishes ($-dp/dr=0$) and calculated Lep is 0.0325. The velocity grows to 98% at the downstream and (z^*=0.136). Kanda and Oshima [10] found the similarity of the velocity distributions above Re 50: Lep=0.045. 0.055, and 0.1 for 98%, 99%, and 100%, respectively. In addition, Leite [18] observed, compared with the calculated results of Boussinesq, that satisfactory agreement existed at the lower Reynolds numbers; however, at higher Reynolds numbers, the formula gave values to be too large for the entrance length. For instance, at Re=13,000, the required length for a satisfactory profile was only 0.8 times the predicted length: Lep=0.052.

The brief results of investigations are summarized in Table 2, where p denotes the pressure and v the radial velocisy.

1.3 Transition Length

We define three types of Reynolds numbers: a transitional Reynolds number, a critical Reynolds number, and the minimum critical Reynolds number. If the speed of the flow along a circular pipe increases, transformation of some individual disturbances into turbulence occurs. With a greater increase in the velocity, the transition takes place more violently. A "transitional Reynolds number" is a Reynolds number at which a transition takes place, and has a wide range of values under the same inlet and experimental conditions. The minimum value of transitional Reynolds numbers is defined as a "critical Reynolds number" under some condition. The numerical value of a critical Reynolds number depends very strongly on the conditions which prevail in the inlet of a pipe, such as the shape of a bellmouth, as well as in the approach of it. As far as is known, there is no upper critical Reynolds number. Ekman reached a value of up to 40,000 [26]. The minimum value of a critical Reynolds number is defined as the "minimum critical Reynolds number", which is approximately 2,000–2,300. Below this value, the flow remains laminar under infinitesimal disturbances.

Experiments for determining the trnsition length have rarely been performed. Instead, most experiments have been carried out in order to observe conditions under which the transition occurs and to determine critical Reynolds numbers and the minimum critical Reynolds number. Moreover, the experiments have often been performed with brass pipes. The transition takes place in a pipe, so the tansition length must be shorter than the pipe length or the distance from the inlet to the measuring point. Of course, the transition does not occur just at the downstream end. Accordingly, we regard a pipe length, or the distance above mentioned, as the transition length when this is not measured.

Transition length<pipe length

or

Transition length<distance from inlet to measureing point

The first investigation was done by Hagen, and he observed that the transition depends on the radius of a pipe, on the velocity, and on the temperature of the water [21]. He used three brass tubes of 0.281, 0.405, 0.596 cm in diameter and 47.6, 108.7, 104.3 cm in length, respectively. We cannot precisely estimate the transition length due to the pipes being of brass. However, the dimensionless transition length can be roughly calculated as less than 0.0734 at Reynolds number 23,000 and less than 0.0241 at Reynolds number 7,000.

Reynolds showed, by dimensional analysis, that the transition depends on the dimensionless expression, that is, the Reynolds number. He conducted experiments 29 times with color bands to obtain the critical velocities at which steady motion breaks down. Reynolds numbers of the experiment vary within 11,500 and 14,400.

The average value is 12,900. He observed that the transition would never occur in the entrance region at less than 30 diameters in any of his pipes. The dimensionless transition length (the minimum critical transition *Re*) by Reynolds is about 0.00233.

Schiller [25] performed his experiments by measuring the pressure drop of a flow of water through smooth cylindrical brass pipes. He showed that the least necessary transition length in order to create an abrupt breakdown of the laminar flow must be not less than 100–130 pipe diameters. He observed the abrupt change in the pressure drop at transition length of 0.039 by using a pipe with sharp edges. Moreover, Schiller [7] conducted experiments by inserting a thin thread of dye into the fluid (see 3.2).

According to the measurements performed by Kirsten [26] the transition length is 50 to 100 diameters. Leite [18] conducted experiments in a Lucite pipe of 1.25 in. in diameter and 73 ft. (700 diameters) long. High-pressure air (90 lb in^2) was used. The peripheral distributions of amplitude of disturbances were measured at points after the disturbance generator which was mainly placed in a fully-developed region. The small disturbances were decayed after 12.4 diameters downstream of sleeve at $Re=13{,}000$: $z^*=12.4/13{,}000=0.00095$. He suggested the significant conclusions (see 3.4). Arakawa and Matsunobu [1], [2] found turbulence at a Reynolds number 2,000 with straight pipes of 1 cm diameter and 17.5 and 35 cm in length. The dimensionless transition length is less than 0.00875. Ramaprian and Tu [22] used a copper tube of 5 cm internal diameter and 880 cm in length. The test section is followed by another copper tube 30 cm long closed at the downstream end and distributions of turbulent velocities were obtained at a Reynolds number of 2870. *Let* is less than 0.0613: $Let<880/(5*2870)=0.0613$. They also observed fully turbulent flow at all times in the case of $Re=2{,}100$ *Let* is below 0.0838. Moreover, no turbulent plug was observed for *Re* below 2,000 by Stettler and Hussain [28], and random puff was recorded at $Re=2{,}100$ and $z/D=330$, where z is a axial length and a pipe diameter D is 2.54 cm. *Let* is below 0.157. Oshima and Kanda [11], [12] carried out color-dye experiments to measure the transition length under two different inlet conditions: (a) without a bellmouth, (b) with a bellmouth. The results are presented in detail in the following section. The results above mentioned are summarized in Table 3.

1.4 Critical Reynolds Number by Stability Analysis

The critical Reynolds numbers according to theory and from observation often widely disagree. The theoretical Reynolds number indicates the point on the wall at which amplification of some disturbances begins. The disturbances flow downstream and the observed point of transition will be downstream of theoretical value. in other words, the experimental critical Reynolds number exceeds its theoretical value. In this paper, however, for reasons of simplicity, neither critical Reynolds number is not distinguished accurately.

Small-disturbance stability theory has been applied several times to Poiseuille flow. Sexl began the theory of the instability of pipe flows for axisymmetric disturbances. Analytical studies have shown that the pipe flow in the fully developed region is stable to small axisymmetric disturbances and also to small non-axisymmetric disturbances [3], [5], [6], [24]. However, Tatsumi [29], by using the boundary-layer approximation

Table 3. Summary of Transition Length

Authors	*Re*	Transi. Length Let (cm)		Bell Mouth	Notes
Arakawa	2000	.0175>	(35)	yes	D=1
Arakawa	3500	.005>	(17.5)	yes	D=1
Kirsten			(50–100)*D		
Leite	13000				large disturbance
Oshima, Kanda	2702	.00234	19	no	D=3
Oshima, Kanda	3766	.000619	7	no	D=3
Oshima, Kanda	6690	.00847	170	8.7×4	D=3
Oshima, Kanda	13473	.00210	85	8.7×4	D=3
Pfenninger	50000				
Ramaprian,	2100	.0838>	880	yes	D=5
Ramaprian,	2870	.0613>	880	yes	D=5
Reynolds	12900	.00233	30*D	yes	D=2.68, 1.527, 0.7886
Schiller		.039		no	
Stettler,	2000	0.165>	838	orifice	D=2.54
Davy, Drazin					axisymmetric
Dixon, Hellums					disturbance profile
Garg, Rouleau	10000>				axisym./non-axisym.
Huang, Chen	39800				axisymmetric
Huang, Chen	39560	.00123			non-axisymmetric
Kuwabara, S	1213				deformed profile
Salwen,	500000>				axisymmetric
Tatsumi	19400	.000375			

and linear stability, calculated numerically a minimum critical Reynolds number for developing laminar flow in the entrance region of a circular pipe: 19,400 at the point 8.5 times the pipe diameter downstream from the inlet (Let=0.000438). Huang and Chen, by linear stability due to axisymmetric [9] and non-axisymmetric disturbances [8], also obtained minimum critical Reynolds numbers 39,800 at Let=0.0008 and 39,560 at Let=0.00123, respectively. These values are much less than the dimensionless entrance length of 0.1. Kuwabara [15] obtained a critical Reynolds number of 1,213 for the fully developed flow by the nonlinear hydrodynamical stability. However, since a mean flow is strongly deformed, his velocity profile appears to belong to that in the entrance region. The brief results of these investigations are summarised in Table 3.

1.5 Numerical Analysis

The references on computational, numerical analyses of hydrodynamic stability are fewer than expected. One of the difficulties of numerical simulation is obtaining the correct, time-dependent solutions for flow at higher Reynolds number. The accuracy of numerical results should always be confirmed. Moreover, it is only with considerable difficulty oscillations of turbulent flow can be distinguished from those of a numerical instability. Dixon and Hellums [4] changed the amplitude of disturbances and estimated the relationship of critical Reynolds numbers and the magnitude of

amplitude. The appearance of distortions in wave form of the vorticity fluctuation are reproducible and give a reasonably well-defined Reynolds number/amplitude relationship. The results show both the strong amplitude dependence of stability and minimum critical Reynolds number of about 2,000. The flow field length is 18.5 times diameter of a pipe. The dimensionless transition length is less than 0.037, 0.00617, 0.00185, 0.000185 at Reynolds numbers of 500, 3,000, 10,000, and 100,000, respectively. Kyrazis [16] constructed a numerical model of Leite's experiment at a Reynolds number of 13,000, utilizing the full, nonlinear, time-dependent Navier-Stokes equations. The calculated disturbance magnitude varied over a 100,000:1 range. For fully developed Hagen-Poiseuille flow: 1) A large disturbance is stable and propagate downstream as if it were an infinitesimal disturbance; 2) Undisturbed Hagen-Poiseuille flow is stable for both small and large disturbances. The first result is against the observation of Leite. Starting with the experimental data of Laufer, Kawamura [13] simulated directly the flow field for a circular pipe by using a three-dimensional explicit scheme. The results of the velocity distributions agree well with the results of Laufer. However, the transition length is ignored.

2. Experiment

The experimental apparatus is shown in Figs. 3 and 4. At the downstream end of the pipe there is a plate with several types of holes which control the amount of flow. After water in a container appears to be steady, fluid enters a smooth circular pipe of 3 cm in diameter and 300 cm in length from a very large container. The bellmouth and pipe are made of acrylic resin and the diameter of the inlet of the bellmouth is 8.8 cm and its central length is 4 cm. The experiments were carried out in two cases: (a) without the bellmouth, (b) with the bellmouth. The main objective of the experiments are to measure the transition length by the color-dye method and to determine conditions under which the transition occurs. The change of color-dye filament in the pipe was observed by several persons. It was difficult to determine the precise transition point because the starting point of oscillation moves a considerable-distance upstream and downstream, and is therefore not clearly distinguishable. We assumed that the transition length is a distance from the inlet to a point where the color-dye filament begins oscillation perpendicular to the main flow.

Table 4 shows the experimental data of the transition length. The importance of reproducibility was well ascertained for the experiment without the bellmouth, but not the one for with the bellmouth. The measured data were for $858<Re<40{,}530$. The Reynolds number was calculated from the total flux.

In the case without the bellmouth, the transition length is about 19 cm for $Re=2{,}702$ ($Let=0.0023$) and 7 cm for $Re=3{,}766$ ($Let=0.00062$). Below $Re=1{,}930$, no transition appears even under manual vibration of the container. In the case with the bellmouth, the transition length is about 170 cm for $Re=7{,}000$ ($Let=0.0081$), between 80 and 120 for $Re=11{,}500$ ($Let=0.0023$–0.0035) and 70 for $Re=15{,}440$ ($Let=0.0015$). Below $Re=5{,}404$, no transition appears even under manual vibration of the container. No special disturbances were used to make the transition occur. The results are

Table 4. Experimental Transition Length

Re	Transition Length (cm)	*Let*	Notes
858	No		No bellmouth
1245	No		
1930	No		
2702	19	0.00234	
3766	7	0.00061	
1061	No		With bellmouth
1206	No		
1351	No		
1673	No		
2027	No		
2059	No		
2895	No		
3989	No		
5404	No		
5790	No		
6690	170	0.00847	
7591	170	0.00746	
8685	117	0.00449	
10315	110	0.00355	
11028	80	0.00241	
11773	120	0.00339	
13473	85	0.00210	
13510	86	0.00212	
13581	70	0.00171	
14036	110	0.00261	
15440	70	0.00151	
15440	105	0.00226	
16192	122	0.00251	
16405	62	0.00125	
18013	91	0.00168	
18142	105	0.00192	
18335	100	0.00181	
20265	85	0.00139	
20864	57	0.00091	
21054	115	0.00182	
23588	68	0.00096	
24347	60	0.00082	
24496	85	0.00115	
26055	82	0.00104	
28073	65	0.00077	
32166	70	0.00072	
32167	55	0.00056	
35090	70	0.00066	
35512	50	0.00046	
40530	43	0.00035	

plotted in Fig. 5 of the following section.

Both *zet* and *Let* become smaller as the Reynolds number is increased.

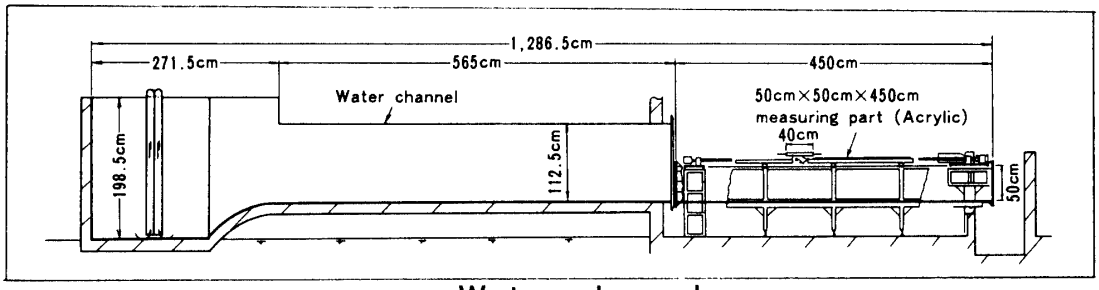

Water channel

Fig. 3. Water channel.

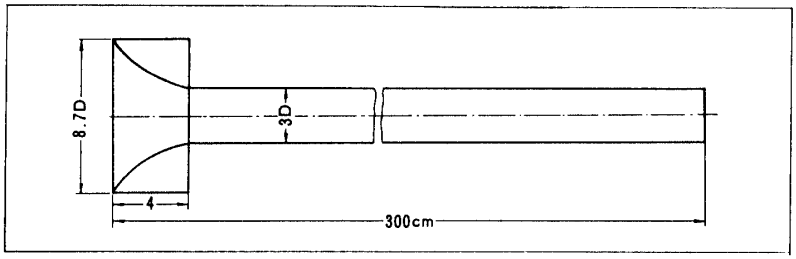

Circular pipe and Bellmouth

Fig. 4. Circular pipe and bellmouth.

3. Problems of Transition

3.1 Stability Theorem of Lord Rayleigh

Here, the problem is clarified and reasonably defined. Lord Rayleigh derived several important, general theorems concerning the stability of laminar velocity profiles, and Tollmien verified these for more general conditions [26]. The validity of these theorems has been confirmed for both inviscid and viscous flows.

1) Theorem 1: The existence of a point of inflection constitutes a necessary condition for the occurrence of instability. Much later, Tollmien showed that it is also a sufficient condition for the amplitude of disturbances.

2) Theorem 2: The velocity of propagation of neutral disturbances in a boundary layer is smaller than the maximum velocity of the mean flow.

3.2 Schiller's Observations on Transition

The problem was studied experimentally by Schiller [7] and the flow could be visualized by inerting a thin thread of dye into the fluid with a small pipette. For Reynolds numbers below 300, the stream line separating the deadwater region from the main flow appears. For Reynolds numbers greater than 1,600–1,700 the inlet flow takes on a new appearance and large, elongated vortices appear in the deadwater region. Schiller and Kurzweg suggested that the onset of turbulence occurred when

$$\frac{D\Gamma}{2\nu} = 1700$$

where Γ is the circulation per unit length near the wall.

3.3 Problems Proposed by Lin

According to Lin [19], most of the research work on the stability of laminar motions has the following final objectives:

1) The first aim is to determine whether a given flow (or a given class of flows) is ultimately unstable for sufficiently large Reynolds numbers. For this purpose, it is desirable to obtain some simple general criterion which will give a rapid classification of velocity profiles according to their stability.

2) The second purpose is to determine the minimum critical Reynolds number at which instability begins. It is often easier to find sufficient conditions for stability than to find the condition for passage from stability to instability.

3) Finally, we want to understand the physical mechanism underlying the phenomena by giving theoretical interpretations and experimental confirmation of the results obtained from mathematical analysis.

3.4 Problems Observed by Leite

Leite's experiments were mostly carried out in the fully-developed region. For that region, some important results on the stability of a circular pipe are stated as follows:

1) Axially symmetric Poiseuile flow was found to damp the small disturbances introduced, whether they be axially symmetric or not, up to a Reynolds number of 13,000.

2) Experimetnal values of rate of decay were found to agree satisfactorily with those given by a recent theoretical analysis, even though assumptions of axial symmetry and longitudinal homogenity of the disturbance are assumed in the latter.

3) To a first approximation, the propagation velocity of the disturbance does not depend upon radial position, hence upon local stream velocity, and is independent of distance downstream.

4) It has been found that small disturbances decay at all Reynolds numbers investigated and that large disturbances are unstable. Therefore, for fixed Reynolds numbers some disturbance of intermediate amplitude must be marginally stable.

3.5 Problems of Transition

Several results of prior experimental and analytical research are summarized graphically in Fig. 5 in such a way that immediate comparison can be easily made. Both dimensionless entrance and transition length are on a log scale. The entrance length is of Schiller, Langharr, Mohanty, Vrentas, and Kanda. Despite the fact that results of Schiller are the smallest among them, the order of each value is nearly the same and the largest dimensionless entrance length is calculated 0.1 by Kanda and Oshima. The experimental data is of Reynolds and Oshima. The relation between two experimental lines seems to depend on the shape and size of a bellmouth. If a smaller bellmouth is used (case A), a graph of experimental data will be plotted between two lines. If a larger bellmouth is used (case B), a graph will be above the line with the bellmouth and shifted to the right. Different critical Reynolds numbers exist under

different experimental apparatus. The transition length is strongly affected by the shape and size of a bellmouth. Without a bellmouth, a critical Reynolds number decreases to the minimum value, that is, the minimum critical Reynolds number. Moreover, for the reproducibility of experimental data, it is very interesting that the results of Reynolds agree well with those of Oshima where a bellmouth was used: $Let=0.00210$ at $Re=13{,}473$. Reynolds experimented by using pipes with bellmouth, too. "The experiments were made on three tubes. The diameters of these were nearly 1 inch, 1/2 inch and 1/4 inch. They were all fitted with trumpet mouthpieces, so that the water might enter without disturbances."

The Reynolds result is $Let=0.00233$ at $Re=12{,}900$, which is very near the line with the bellmouth. Moreover, it was found that all of the experimental transition lengths are shorter than any of the entrance lengths in a dimensionless form in Fig. 5. In addition, the results of stability analysis of Tatsumi and Huang are presented together in Fig. 5. The patterns seen in the down half of their curves are similar to the graphs of experimental data. As the Reynolds number increases, the dimensionless transition

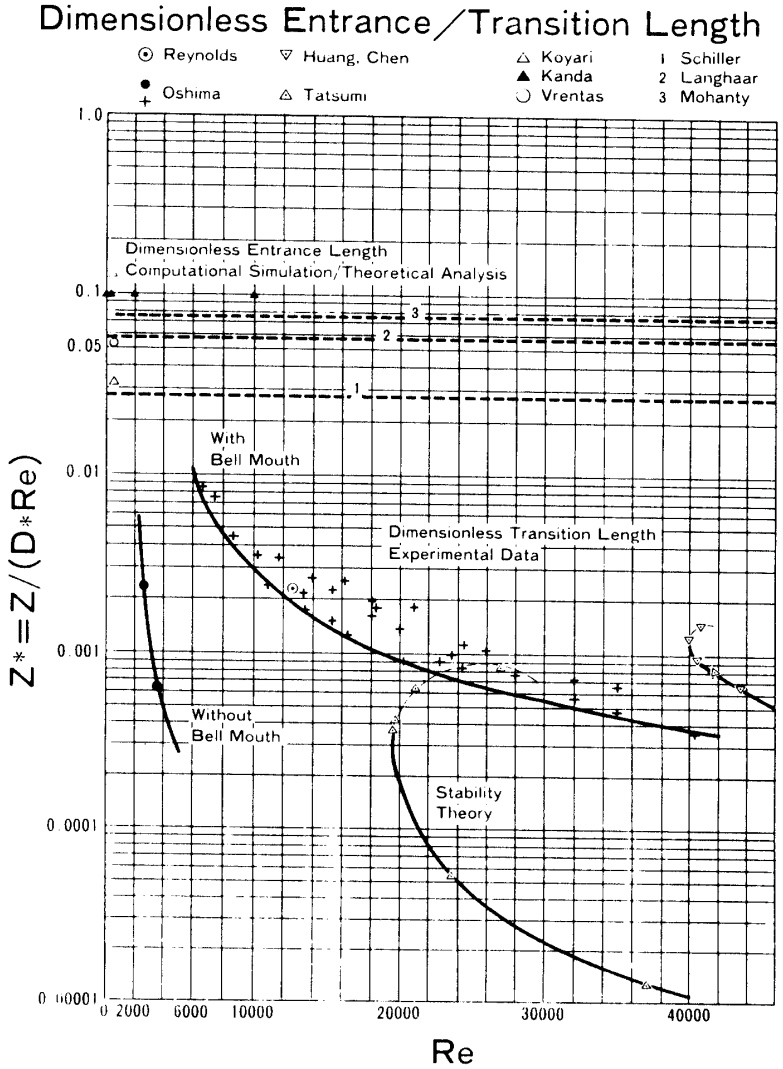

Fig. 5. Entrance and transition length.

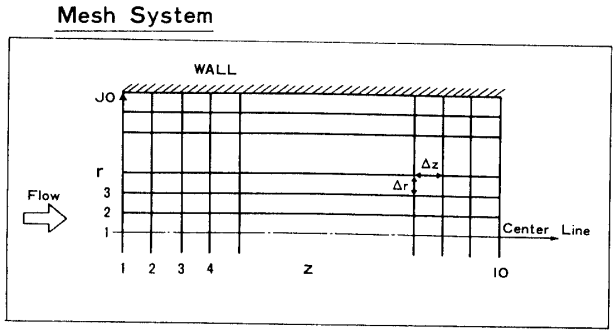

Fig. 6. Mesh system.

length becomes shorter. The results of Tatsumi and Huang correspond to case A and B, respectively, and also smaller than the dimensionless entrance length.

As a result of the above discussion we must conclude the problem of the transition as follows:

1) The transition occurs in the entrance region. The transition length becomes shorter as the Reynolds number increases under the same experimental condition.

2) A critical Reynolds number depends on an experimental apparatus, especially on the shape of a bellmouth, provided not external nor manual disturbances are given to the upstream and inlet conditions.

3) The minimum critical Reynolds number exists for infinitesimal disturbances (i.e., a case without a bellmouth).

4. Numerical Simulation

4.1 Mesh System and Basic Equations

The rectangular mesh system used is schematically shown in Fig. 6. Subscripts IO and JO are the number of axial and radial grid points, respectively. Axial indexes $I=1$ and IO mean the inlet and outlet of a pipe. Radial indexes $J=1$ and JO denote the center line and wall of a pipe. The mesh spacing dz and dr are each constant and the aspect ratio of dz to dr is 1 for cases of $Re=10{,}000$ or 2 for $Re=2{,}700$ in order to catch mesh-size disturbances. We could not simulate the turbulent flow field when using a larger aspect ratio of 500 for a case of $Re=10{,}000$ [10], and steady solutions are obtained.

The two-dimensional, stream-function vorticity equation and the Poisson equation are applied to simulation of appearance of turbulence in the entrance region of a circular pipe. We consider an incompressible Newtonian fluid with constant viscosity and density and neglect gravity and external forces.

Stream-function vorticity equation in the cylindrical coordinates:

$$\frac{\partial \omega}{\partial t}-\frac{1}{r}\frac{\partial \psi}{\partial z}\cdot\frac{\partial \omega}{\partial r}+\frac{1}{r}\frac{\partial \psi}{\partial r}\cdot\frac{\partial \omega}{\partial z}+\frac{\omega}{r^2}\frac{\partial \psi}{\partial z}=\frac{1}{Re}\left\{\frac{\partial}{\partial r}\left(\frac{1}{r}\frac{\partial}{\partial r}(r\omega)\right)+\frac{\partial^2 \omega}{\partial z^2}\right\}$$

Poisson equation:

$$-\omega=\frac{\partial}{\partial r}\left(\frac{1}{r}\frac{\partial\psi}{\partial r}+\frac{\partial^2}{\partial z^2}\left(\frac{\psi}{r}\right)\right.$$

These equations are time-dependently solved by the iterative Gauss-Seidel method.

There is no fundamental reason why one should not be able to simulate a turbulent flow in any desired detail. The Navier-Stokes equations are believed to be a sufficient description, and discretization errors can in principle be made as small as one wishes. However, it is difficult to simplify and summarize the enormous volume of results produced. The convergence of iterative methods is affected by several parameters, such as the Reynolds number, mesh spacing, time increment, and especially the iteration convergence criteria.

One of the most interesting problems concerns the selection of appropriate conditions for the inlet boundary. In this paper, simulations for large disturbances are discussed. We can roughly estimate the characterictics of the flow field from the result of vorticity and velocity profile. For smaller disturbances, the results will be presented in detail in the subsequent chapter. The initial and boundary disturbances are given as follows:

1) First, the stream function is given as all the fluid particles start moving downstream with uniform velocity (Eq. (5)).

2) Values of the stream-function are multiplied by an amplitude constant for points of $2dr$, $3dr$, and $4dr$ apart from the wall. These points are at $r=0.45$, 0.425, and 0.4. (Eq. (6)). Thus, the velocities of fluids near the wall are larger than those in the central core.

3) After starting (time$=dt$), the same disturbances at the inlet remain constant, but the initial disturbances of other points are freed. Stream-function for these points are calculated according to a scheme (Eq. (7)).

$$\psi(i,j)=\left(\frac{j-1}{JO-1}\right)^2 \quad \text{for } i=1,\ IO \text{ and } j=1,\ JO$$

$$\psi(i,j)=\psi(i,j)*f \quad \text{for } i=1,\ IO \text{ and } j=JO-2,\ JO-3,\ JO-4$$

$$\psi(1,j)=\psi(1,j)*f \quad \text{for } j=JO-2,\ JO-3,\ JO-4$$

where f is an amplitude constant.

For smaller disturbances, the amplitude constant and number of stressed grid points will be decreased accordingly. We do not know precisely the magnitude of infinitesimal disturbances of real flows. For example, Leite measured the mean amplitude of axial component of small residual disturbances and found that it had a maximum value of approximately 10^{-4}. These disturbances were believed to be largely caused by radial sound, because their amplitudes varied little across the pipe.

The simulation of disturbed flow fields is performed for three cases, as seen in Table 5.

Table 5. Simulation Case

Reynolds Number	Disturbance			Time	*dz/dr*
	Name	Point (i, j)	factor		
2700	2A*1.005	(1,19),(1,18)	1.005	2200*dt*	2
10000	3A*1.1	(1,19),(1,18),(1,17)	1.1	370*dt*	1
10000	2A*1.01	(1,19),(1,18)	1.01	500*dt*	1

Time increment is 0.01 for cases of Reynolds numbers of 2,700 and 10,000. It is made dimensionless by dividing by (R/UO), where R is the radius of a pipe. 2A*1.005 denotes that 1.005 times stream function are assigned to two points.

4.2 Effect of Disturbances at Re=2,700 (2A*1.005)

The flow field in the entrance region is simulated at a Reynolds number of 2,700. A small disturbance of 0.5% of a stream function is added to two points: r=0.045, 0.425 and z^*=0.

Iteration convergence did not attain an acceptable solution to the discretised difference equations after time=2,473*dt*. The differences of the vorticity between iteration k and $k+1$ do not fall within tolerance despite many iterations at time=2,474*dt*. The results at time=2,200*dt* are mainly discussed.

4.2.1 Effect of Disturbances upon Velocity Development

The velocity developments along a pipe are shown in Figs. 7 (a)–(d) for r=0.475, 0.45, 0.35, and 0. The wall and center line are at r=0.5 and 0, respectively. The velocity distributions in the central core (r=0.35 and 0) oscillate cosiderably, although those near the wall (r=0.475 and 0.45) appear to still remain laminar. Fig. 7 (c) shows that the fluctuation of the velocity at r=0.35 begins at about z^*=0.0005 (27*dz*). That at the center line is a little delayed in the beginning (z^*=0.0007 (38*dz*)) from Fig. 7 (d). The amount of amplification decays rapidly after z^*=0.003 (162*dz*). This does not mean that the flow changes from turbulent to laminar after that point. Rather, this is because the inlet disturbances are carried approximately 162*dz* downstream for 2,200 time-steps of computation, and not transferred after 163*dz* down stream point. Unfortunately, the computation cannot develop further under the given iteration convergence criteria.

Supposing the velocity of propagation of neutral disturbances are defined as,

$$\text{Velocity of perturbation of neutral disturbances} = \frac{\text{time}}{\text{axially disturbed length of flow field}}$$

its value is calculated from Figs. 7 (c) and (d).

$$\frac{162\,dz}{2200\,dt} = 0.736$$

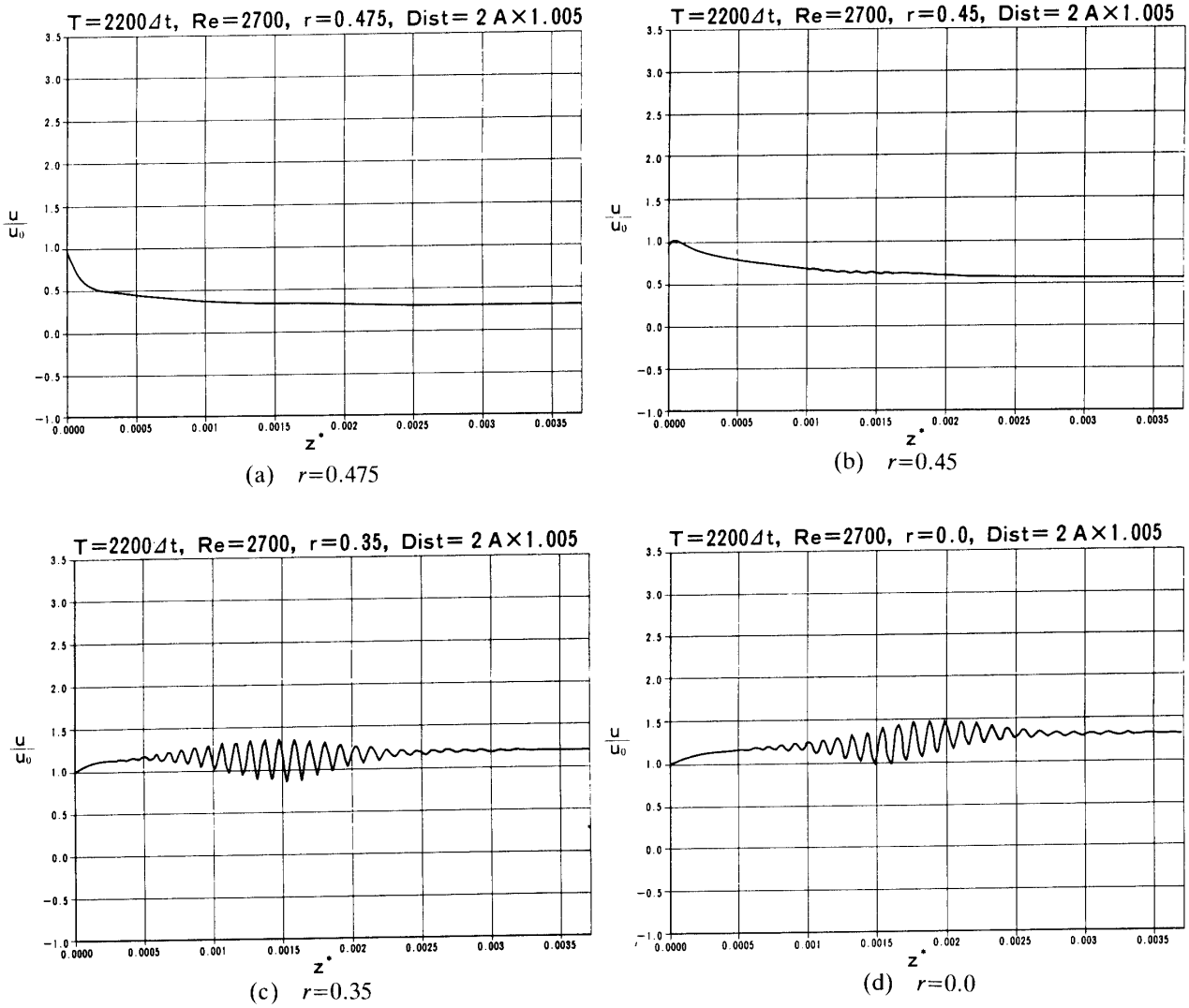

(a) r=0.475 (b) r=0.45

(c) r=0.35 (d) r=0.0

Fig. 7. Velocity development, Re=2700, time=2200dt, Dist=2A*1.005

where space and time increments, and aspect ratio are 1/20, 0.01,and 2, respectively, and a maximum velocity is about 1 in a dimenionless form. This result seems to be reasonable for Rayleigh's Theorem 2 (see 3.1).

Figs. 8 (a)-(b) also display the veocity development at time=2,469dt. The separation point on the wall can be clearly seen at z^*=0.00185 (100dz) in Fig. 8 (a) and sharp back flow is observed at the same longitudinal distance in Fig. 8 (b). These values are only a little smaller than the experimental value of 0.00234 from Table 3. The order of both values, however, are nearly the same. The error is −20.9%.

Compared to a case without any disurbance, the velocity developments at r=0.475 and 0.35 are displayed in Fig. 9. These lines develop smoothly without oscillating. the average value of Fig. 7 (c) is, of course, equal to that in Fig. 9 (r=0.35).

4.2.2 Effect of Disturbances upon Velocity Distribution

Figs. 10 (a)-(g) display how the velocity distribution is influenced by the inlet disturbances over cross sections perpendicular to a longitudinal direction: z^*=0,

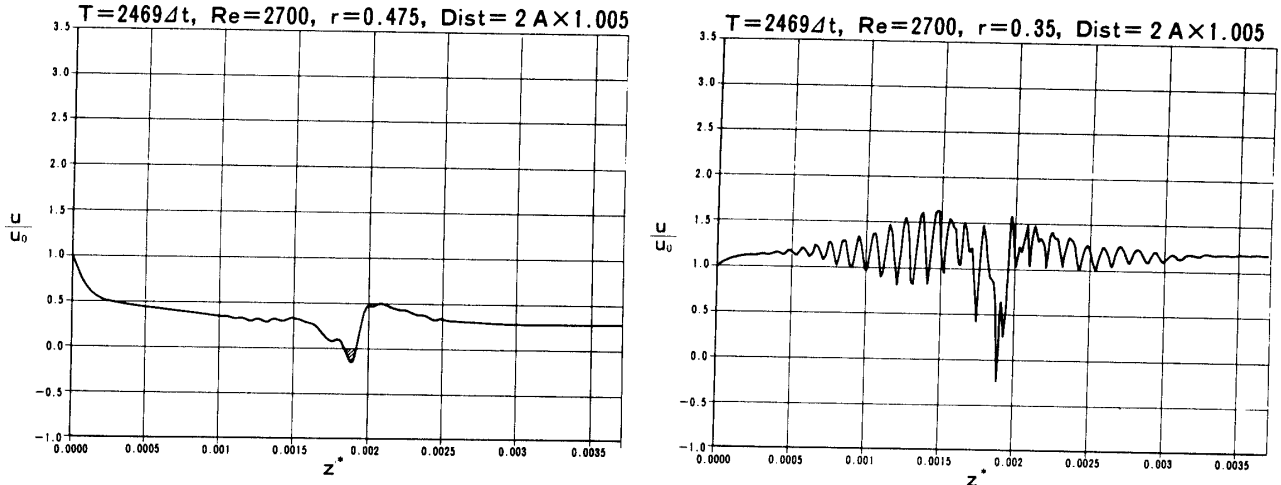

(a) r=0.475 (b) r=0.35

Fig. 8. Velocity development, Re=2700, time=2469dt, Dist=1A*1.005

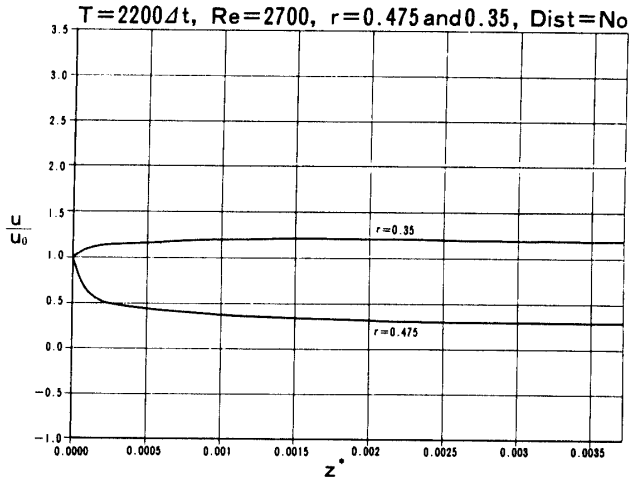

Fig. 9. Velocity development, Re=2700, time=2200dt, Dist=No

0.000259 (14dz), 0.000759 (41dz), 0.0015 (81dz), 0.00185 (100dz), 0.002 (108dz), and 0.003 (162dz), respectively. The separation point on the wall exists near z^*=0.00185 from Fig. 8 (a). The velocity fluctuations given as initial and boundary conditions are shown in Fig. 10 (a), and are not too much larger than expected. Larger fluctuation is given in 4.3.2. The velocity distribution starts waving up and down after z^*=0.000759 in Fig. 10 (c), although it develops in a laminar state until about 0.0007 from Fig. 7 (c). Further downstream in Fig. 10 (g), the velocity distribution regains a laminar flow. The highest value of a periodically varying velocity is seen at about z^*=0.00185 in Fig. 10 (e). The trend of a varying, axial velocity is well understood, even though its value is considerably higher than that of a real flow. The inflection point, which is a necessary condition for the occurrence of instability (Rayleigh's Theorem 1), is not still perceived clearly near the wall. On the contrary, it exists in the central core, as shown in Fig. 10 (e).

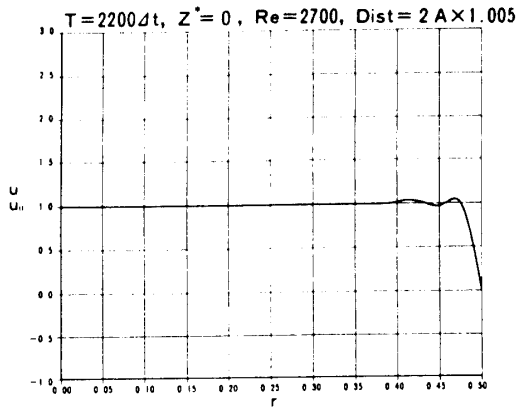

(a) $z^*=0.0$ $(0dz)$

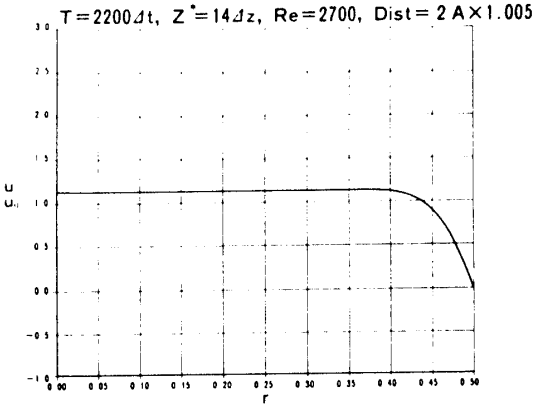

(b) $z^*=0.000259$ $(14dz)$

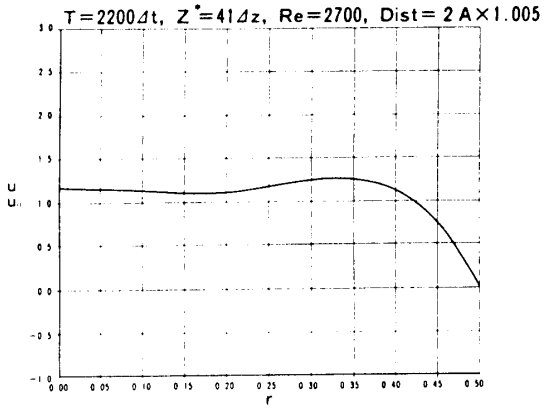

(c) $z^*=0.000759$ $(41dz)$

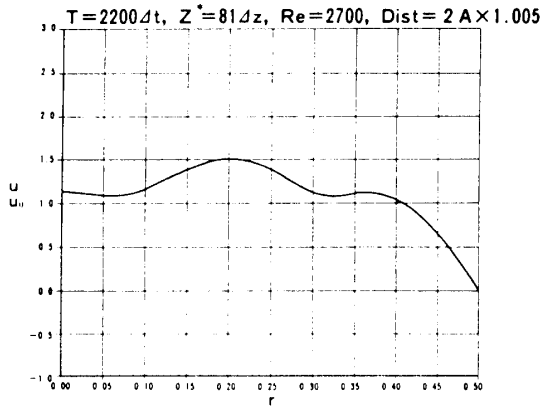

(d) $z^*=0.0015$ $(81dz)$

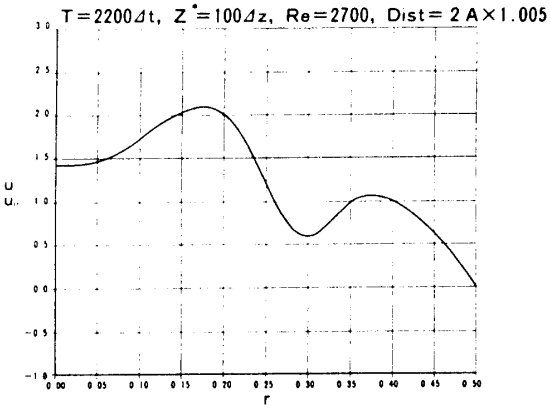

(e) $z^*=0.00185$ $(100dz)$

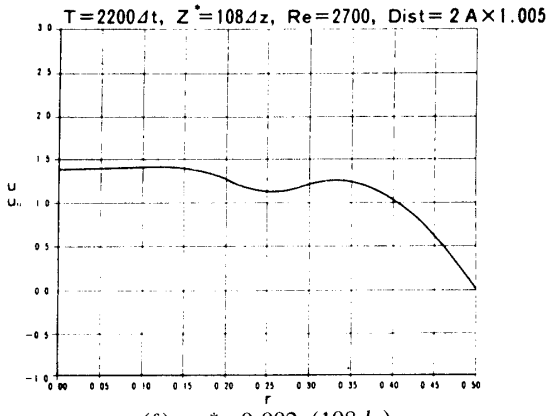

(f) $z^*=0.002$ $(108dz)$

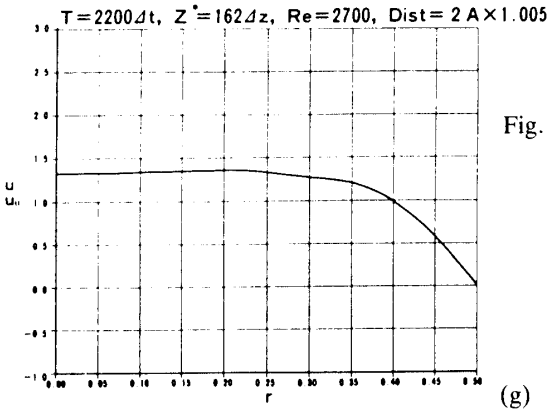

(g) $z^*=0.003$ $(162dz)$

Fig. 10. Velocity distribution, Re=2700, time=2200dt, Dist=2A*1.005

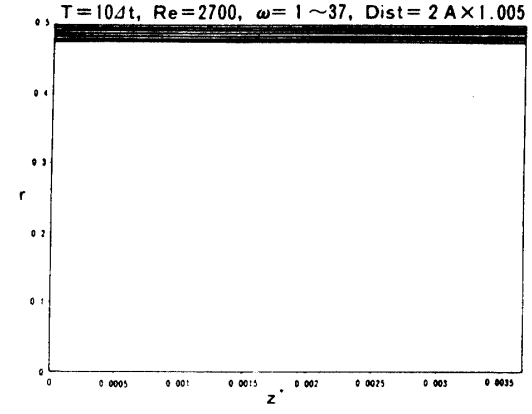

(a) time=10*dt*

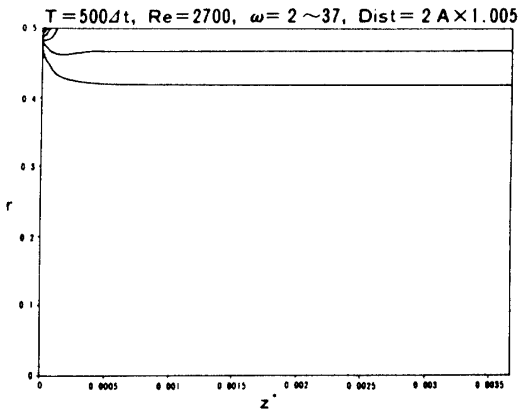

(b) time=500*dt*

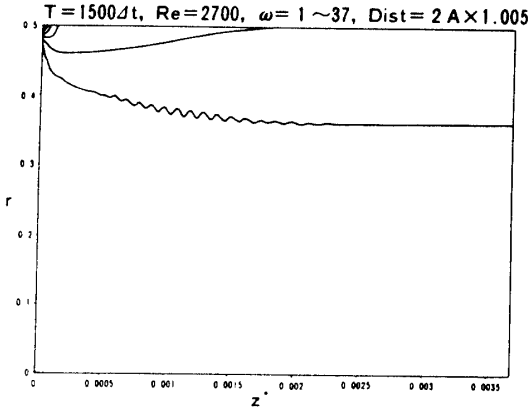

(c) time=1500*dt*

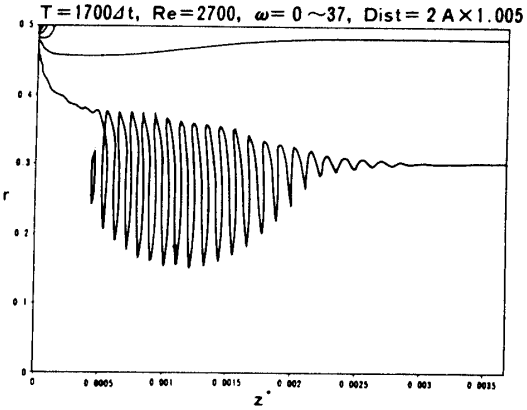

(d) time=1700*dt*

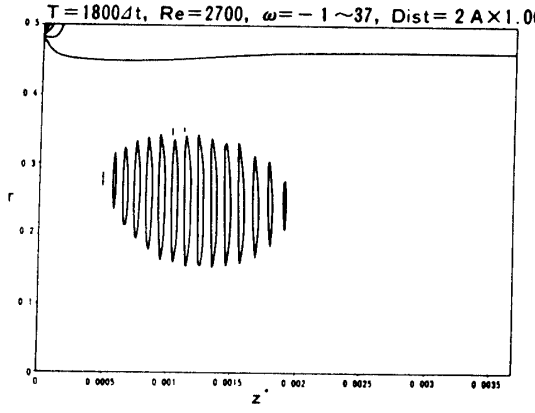

(e) time=1800*dt*

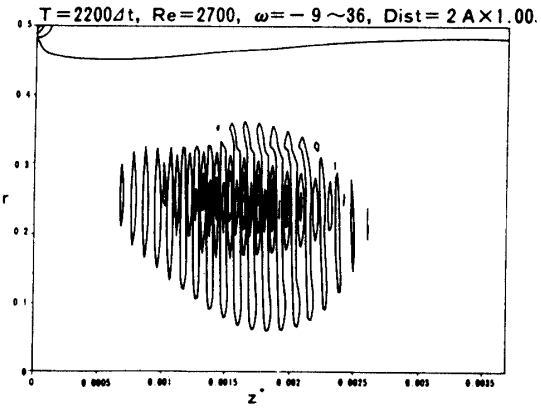

(f) time=2200*dt*

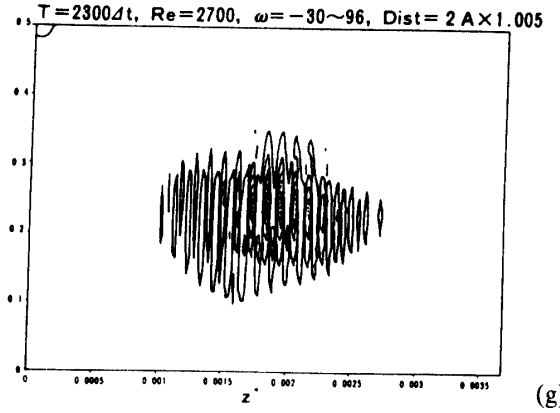

(g) time=2300*dt*

Fig. 11. Vorticity, *Re*=2700, Dist=2A*1.005

4.2.3 Effect of Disturbances upon Vorticity

Vorticity is made dimensionless by dividing by (UO/R).

Figs. 11 (a)-(g) display the distribution of vorticity in the entrance region of a circular pipe through time, for time=$10dt$, $100dt$, $200dt$, $300dt$, $350dt$, and $370dt$, respectively. In general, the vorticities near the wall are stronger than those in the central core before time=$2{,}200dt$ and their value lies between -9 and 37. The reverse vorticity appears only after time=$2{,}200dt$. The inlet disturbances produce stronger vorticities in the central core than near the wall in Fig. 11 (g). The residual errors for the vorticity become larger with time until convergent solutions cannot be obtained. They are much amplified around the small region after time=$2{,}300dt$, where the dimensionless axial length z^* is about 0.0018 in Fig. 11 (g). The disturbances used have a strong influence on the vorticity of this region. Figs. 11 (c)-(e) shows explicitly how the vorticities are carried to the central part. A vorticity line with equal strength separates from the wall to the central core, then it turns round and round, and finally it breaks into many pieces of vorticity.

4.3 Effect of Larger Disturbances at Re=10,000 (3A*1.1)

The flow field is simulated at a high Reynolds number of 10,000. The 10% increased values of a stream function are supposed at three points: r=0.045, 0.425, 0.4 and z^*=0. These disturbances are considerably larger than in 4.2. Iteration convergence did not attain an acceptable solution after time=$370dt$ and results are saved on a disk-file every $10dt$. Accordingly, the velocity distributions at time=$350dt$ are presented. We can roughly extrapolate, from Fig. 5, that a dimensionless transition length is about 0.00006 to 0.0001 at Re=10,000. Its value corresponds to 1.8 to 3 cm in the case of a pipe of 3 cm in diameter and without a bellmouth. A flow changes from laminar to turbulent very near the inlet of a pipe at Reynolds numbers of above 10,000.

4.3.1 Effect of Disturbances upon Velocity Development

The development of the axial velocity fields are illustrated in Figs. 12 (a)-(d) for several radii: r=0.475, 0.45, 0.35, and 0.25, respectively. In general, the amount of amplification decays rapidly after z^*=0.00015 ($60dz$).

$$\text{Velocity of propagation of neutral disturbances} = \frac{60\,dz}{350\,dt} = 0.857$$

This result seems to be reasonable for Rayleigh's Theorem 2. Fig. 12 (a) shows the velocity development at one dr away from the wall (r=0.475). There are three separation points on the wall, z^*=0.0000225 ($9dz$), 0.0000325 ($13dz$), and 0.000045 ($18dz$). The value for z^*=0.0000325 is the largest among them. Similarly, a big backflow also can be seen at z^*=0.000025 ($10dz$) in Fig. 12 (b). These values are about one third of the extrapolated value of the experimental data in Fig. 5 (about 0.00006 to 0.0001). The order of both values, however, is nearly the same. The error is -62.5%. These disturbances affect considerably the velocity at r=0.35 in Fig. 12 (c),

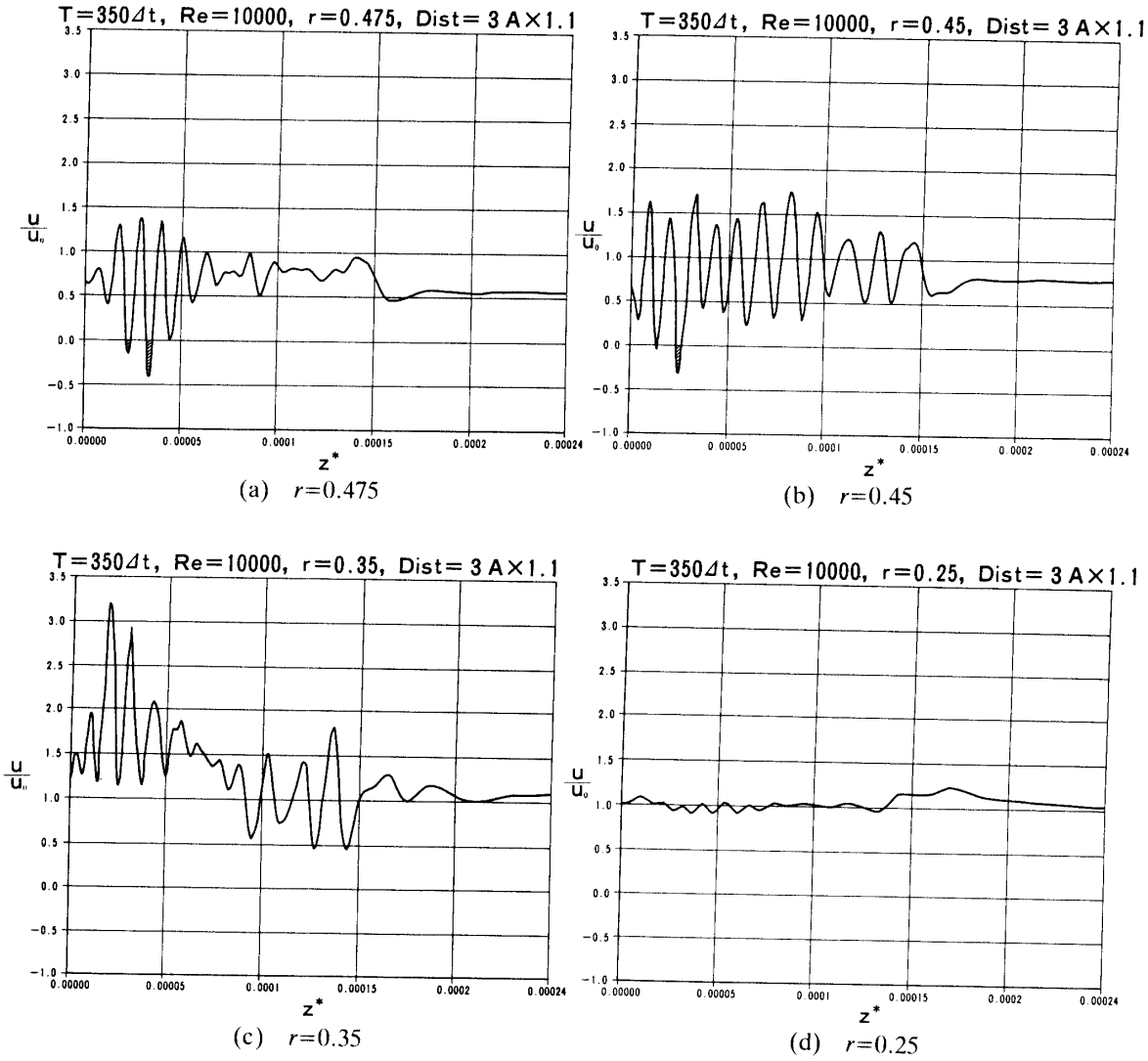

(a) r=0.475 (b) r=0.45

(c) r=0.35 (d) r=0.25

Fig. 12. Velocity development, Re=1000, time=350dt, Dist=3A*1.1

but do not yet influence the velocity at r=0.25 in the more central core in Fig. 12 (d). The velocity fluctuation is the largest at 0.35 among them.

4.3.2 Effect of Disturbances upon Velocity Distribution

Figs. 13 (a)-(g) display how the velocity distribution grows under the inlet disturbances over cross sections perpendicular to a longitudinal direction: z^*=0, 5dz, 9dz, 10dz, 11dz, 50dz and 98dz, respectively. The velocity fluctuation, given as initial and boundary conditions, is shown in Fig 13 (a), and are similar to that at z^*=98dz in Fig. 13 (g) since the disturbances do not grow after z^*=60dz. The amount of fluctuation still remains larger at z^*=50dz in Fig. 13 (f) than at the inlet in Fig. 13 (a). On the other hand, the velocity distributions without any disturbances are displayed for z^*=0 and 0.0000025 (10dz) in Fig. 14, and both lines show that a flow is in a laminar state. Backflows are also shown at z^*=0.0000225 (9dz) and 0.000025 (10dz)

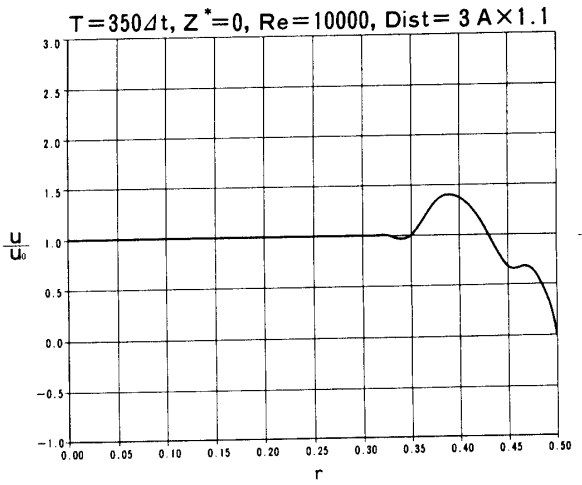

(a) $z^*=0.0$ $(0dz)$

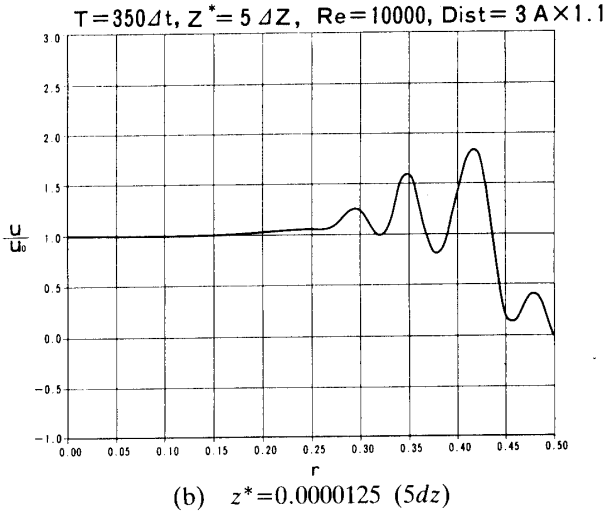

(b) $z^*=0.0000125$ $(5dz)$

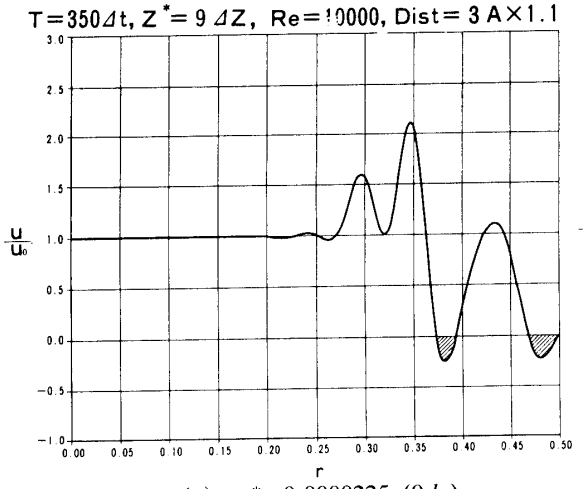

(c) $z^*=0.0000225$ $(9dz)$

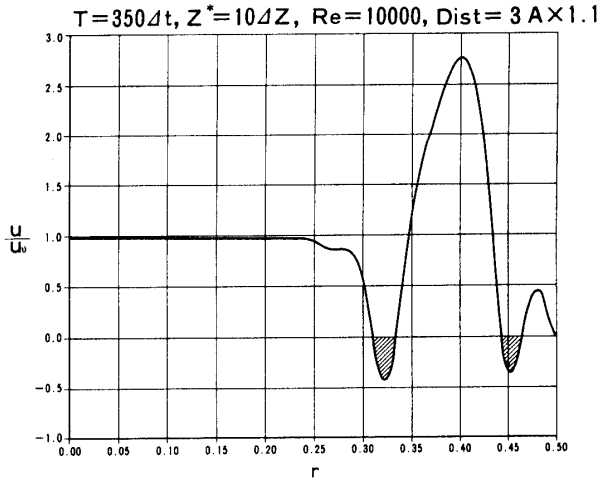

(d) $z^*=0.000025$ $(10dz)$

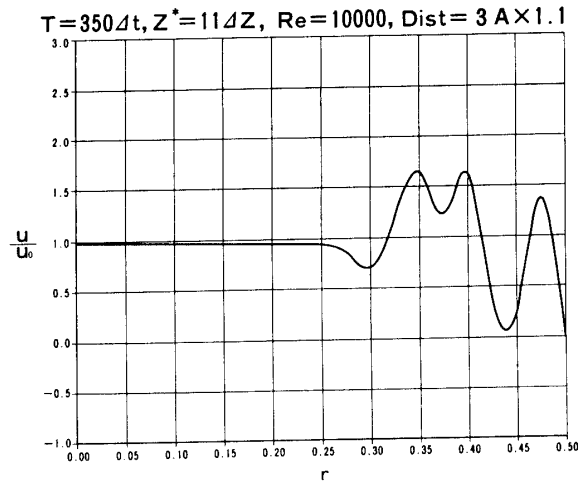

(e) $z^*=0.0000275$ $(11dz)$

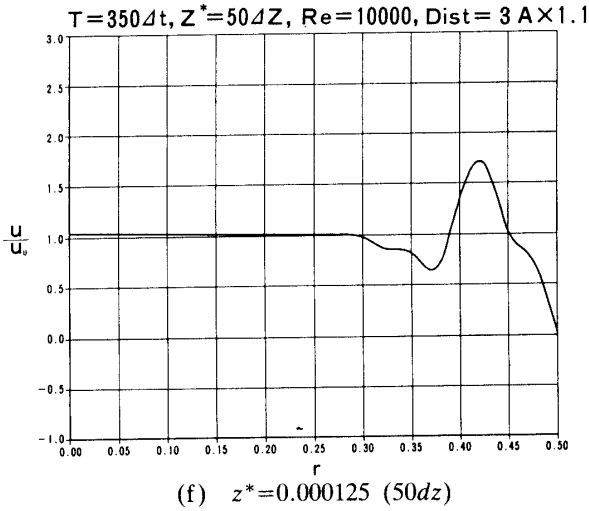

(f) $z^*=0.000125$ $(50dz)$

in Fig. 13 (c) and (d), respectively, even though the amount of fluctuation is considerable in Fig. 13 (d). The velocity profile near the wall shows the existence of an inflexion point at $z^*=5dz$ (0.0000125) in Fig. 13 (b), which is a necessary condition for the occurence of instability (Rayleigh's Theorem 1).

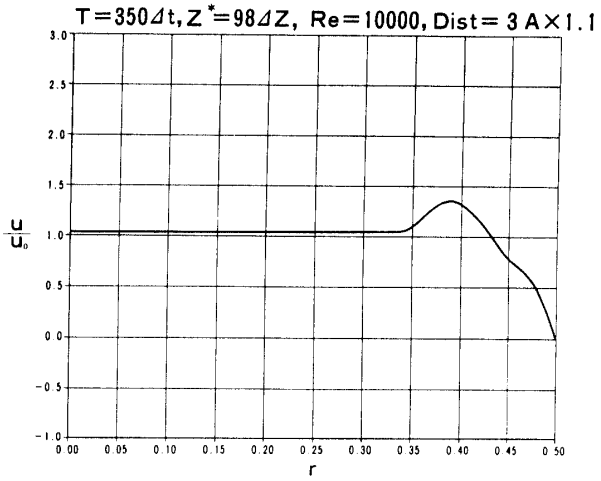

(g) $z^*=0.000245$ ($98dz$)

Fig. 13. Velocity distribution, $Re=1000$, time=$350dt$, Dist=3A*1.1

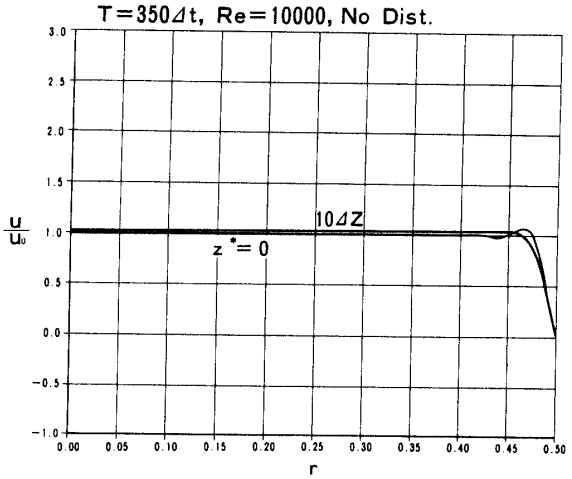

Fig. 14. Velocity distribution, $Re=1000$, time=$350dt$, $z^*=0.0$ ($10dz$) and 0.000025 ($10dz$), Dist=No

The initial fluctuation in Fig. 13 (a) appears to be considerably larger than that in a real flow, since it is about 1.4 times as large as in Fig. 14.

4.3.3 Effect of Disturbances upon Vorticity

Figs. 15 (a)-(f) display the transfer of vorticity for time=$10dt$, $100dt$, $200dt$, $300dt$, $350dt$, and $370dt$, respectively. The value of vorticities is between -11 and 36 before time=$200dt$, then its absolute value increases and reaches between -976 and 1,454 at time=$370dt$ in Fig. 15 (f). However, the value at time=$350dt$ (-184 to 304) does not greatly exceed the average value before time=$200dt$. The residual errors for the vorticity are amplified around the small region at $z^*=0.00003$ and time=$370dt$. The disturbances used have a strong influence on the vorticity at about $z^*=0.00003$. Fig. 16 displays the vorticity in the case of no disturbance at $370dt$, which shows a steady

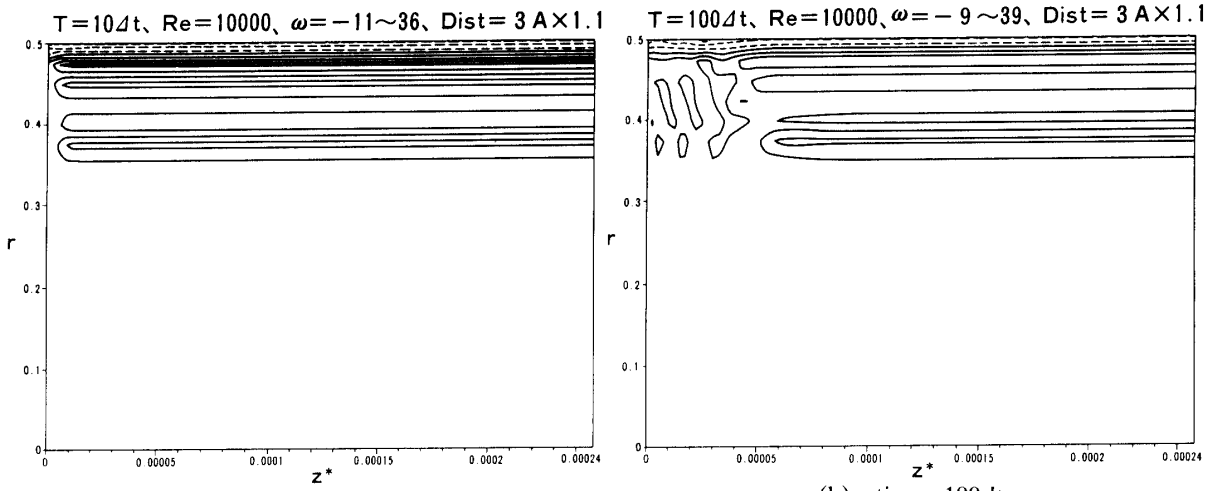

(a) time=10*dt* (b) time=100*dt*

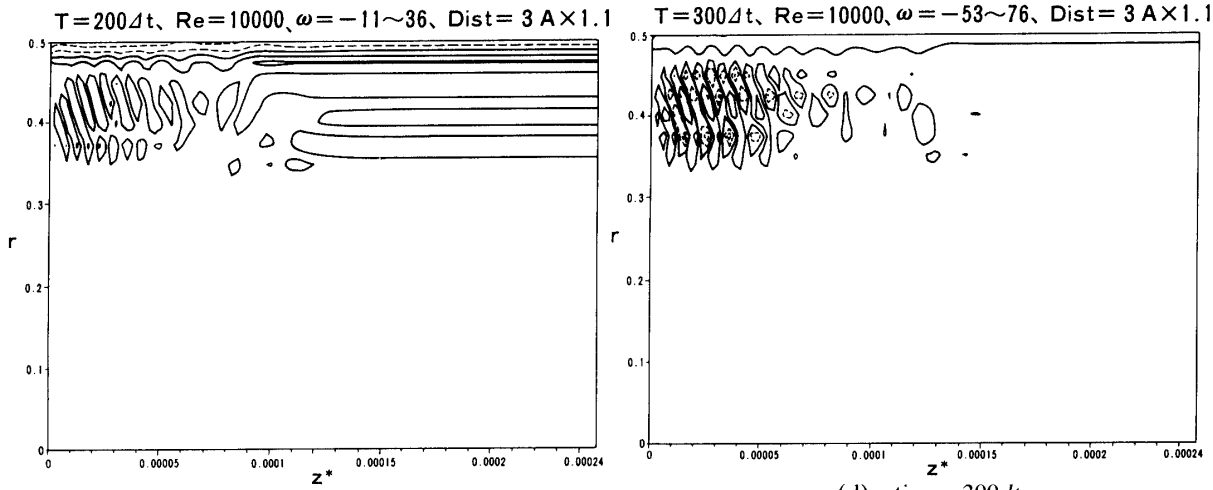

(c) time=200*dt* (d) time=300*dt*

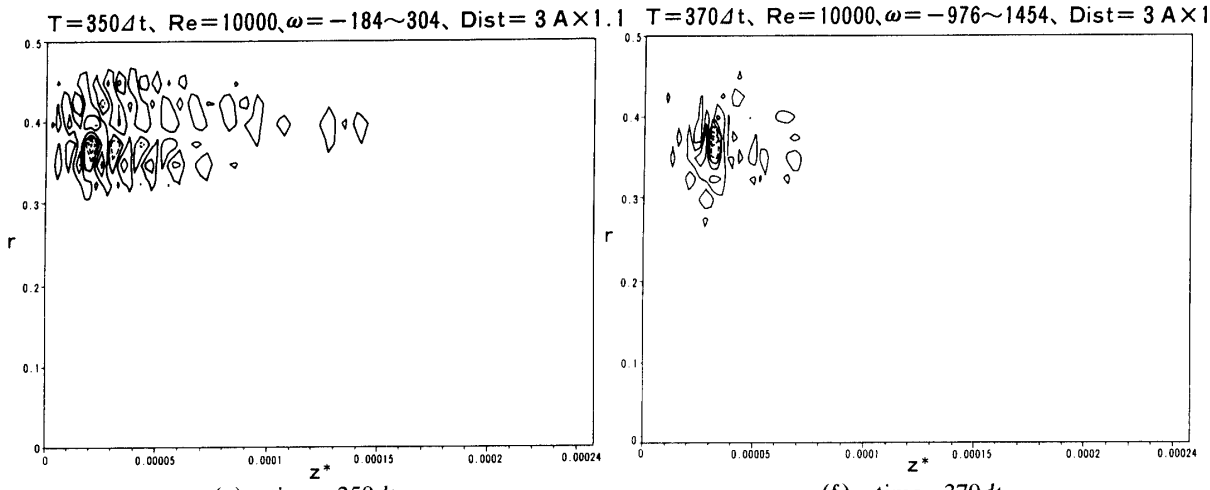

(e) time=350*dt* (f) time=370*dt*

Fig. 15. Vorticity, *Re*=10000, Dist=3A*1.1

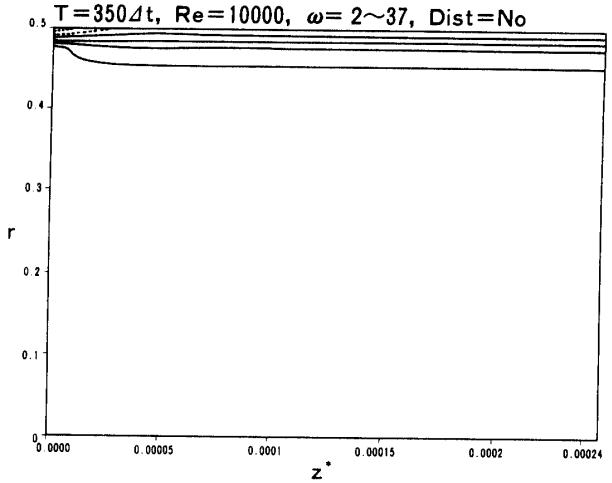

Fig. 16. Vorticity, Re=10000, time=370dt, Dist=No

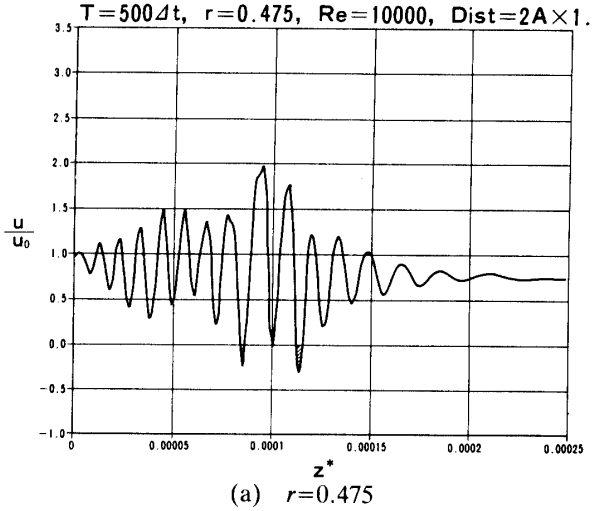

(a) r=0.475

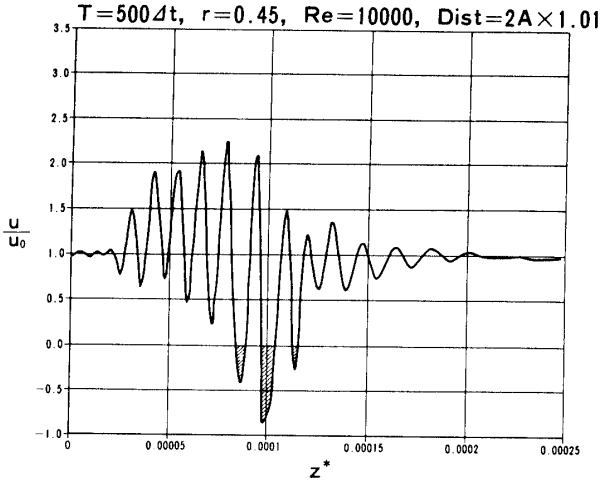

(b) r=0.45

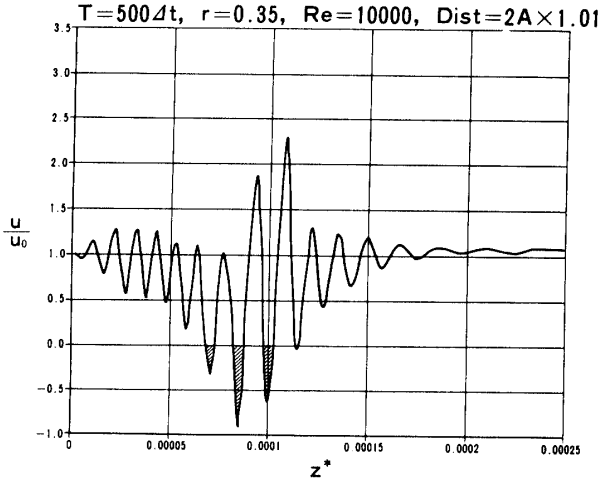

(c) r=0.35

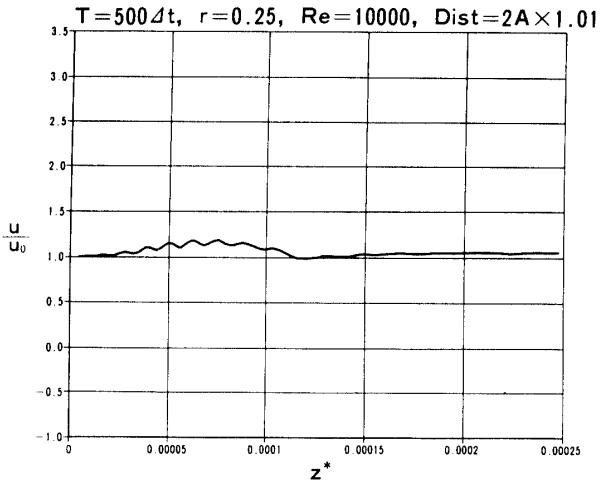

(d) r=0.25

Fig. 17. Velocity development, Re=10000, time=500dt, Dist=2A*1.01

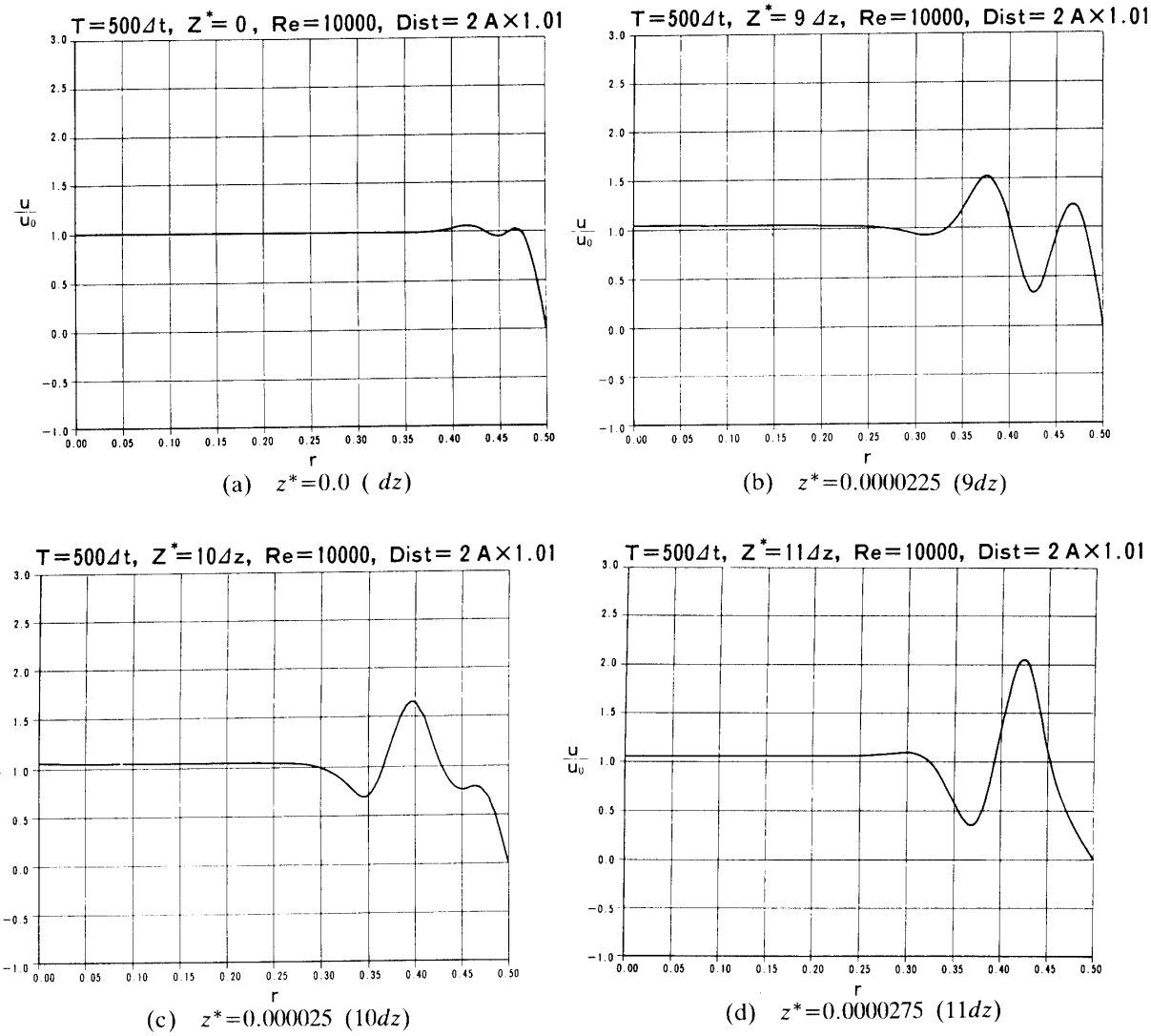

(a) $z^*=0.0$ (dz) (b) $z^*=0.0000225$ ($9dz$)

(c) $z^*=0.000025$ ($10dz$) (d) $z^*=0.0000275$ ($11dz$)

Fig. 18. Velocity distribution, Re=10000, time=500dt, Dist=2A*1.01

and laminar development of the flow field.

4.4 Effect of Smaller Disturbances at Re=10,000 (2A*1.01)

When the convergence criteria are better selected, doubtlessly the calculation step of the simulation will become longer. A smaller disturbance also makes a computation step longer. Initial and boundary disturbances can be easily controlled by an amplitude constant. Here, as a disturbance smaller than 10% in 4.3, the 1% increased stream function is given at the same two points as in 4.2: r=0.045, 0.0425 and z^*=0.

Iteration convergence did not continue after time=500dt, but it is longer than 370dt in 4.3.

4.4.1 Effect of Disturbances upon Velocity Development

Figs. 17 (a)-(d) display the velocity development along a pipe for r=0.475, 0.45, 0.35, and 0.25 at time=500dt. The velocity distribution oscillates violently near the wall at r=0.475 to 0.35. On the contrary, however, it does not swing up and down with

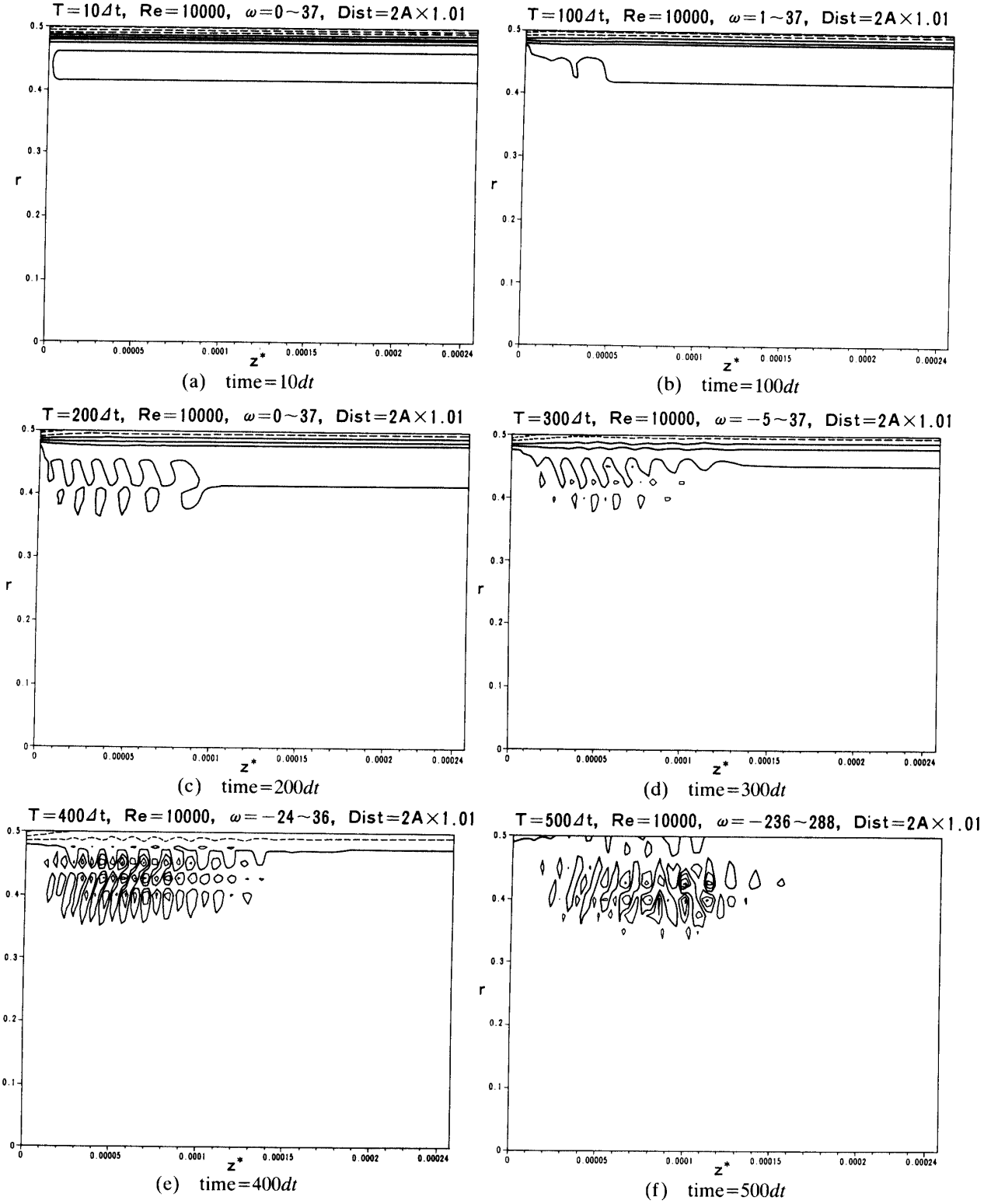

(a) time=10*dt* (b) time=100*dt*

(c) time=200*dt* (d) time=300*dt*

(e) time=400*dt* (f) time=500*dt*

Fig. 19. Vorticity, *Re*=10000, Dist=2A*1.01

a regular motion near the central core at r=0.25 in Fig. 17 (d). This shows that iteration convergence does not arrive at a solution of finite-difference equations before the disturbances are transported to the central core. Fig. 17 (a) express clearly

the separation points at $z^*=0.000085$ ($34dz$), 0.0001 ($49dz$), and 0.0001125 to 0.000115 (45–46dz). The dimensionless transition length agrees fairly well with the experimental value of 0.00006 to 0.0001 and is about four times as large as in 4.3. Figs. 17 (b)-(c) also show big back-flows near the wall. The amount of fluctuation decays after $z^*=0.0002$ ($80dz$).

$$\text{Velocity of propagation of neutral disturbances}=\frac{80\,dz}{500\,dt}=0.8$$

This result satisfies Rayleigh's Theorem 2.

4.4.2 Effect of Disturbances upon Velocity Distribution

Figs. 18 (a)-(d) display velocity distribution over cross sections for $z^*=0$, $9dz$, $10dz$, and $11dz$, respectively. The velocity fluctuation, given as initial and boundary conditions, is shown in Fig. 18 (a). Its value is nearly equal to that in Fig. 10 (a), although the amplitude constant is 1.005 for the latter. Figs. 18 (b)-(d) are compared with Figs. 13 (c)-(d), respectively. The separation points already exist at $z^*=0.000025$ in Figs. 13 (c). However, in the case of smaller disturbances, those appear more downstream first at $z^*=0.000085$. We can see an inflection point near the wall in Fig. 18 (d).

4.4.3 Effect of Disturbances upon Vorticity

Figs. 19 (a)-(f) display the vorticity distribution in response to smaller amplitude disturbances. Vorticities are carried more downstream than in Fig. 15 (f). The vorticity starts flowing downstream at about $z^*=0.00002$ in Fig. 19 (f) and its value increases with this downstream flow; this result meets more natural conditions than that of Fig. 15 (f). The highest value lies at about $z^*=0.001$.

5. Conclusions

The flow field of a circular pipe was studied especially within the entrance and transition region. The results of this study show that a numerical, finite-difference method can simulate development of the Hagen-Poiseuille flow and transition to turbulent flow. The conclutions are:

1) The turbulence transition occurs only within the entrance region.

2) The transition length decreases as the Reynolds number increases under the same inlet conditions.

3) A good bellmouth lessens disturbances at the inlet and the critical Reynolds number becomes larger.

4) The transition was numerically simulated on the condition: a) The aspect ratios of the rectangular mesh system used are 2 for $Re=2{,}700$ and 1 for $Re=10{,}000$ and b) The disturbance is given at the point very near the wall of the inlet.

5) The result of simulation satisfies two theorems of Lord Rayleigh: dependence of the flow stability on laminar velocity profiles.

6) The transition length depends on the magnitude of the disturbance assumed. The transition length obtained numerically is a little shorter than the experimental data, but considered fairly reasonable since the order of the values are the same, and the disturbance for calculation is supposed to be larger than actual ones. In the case of smaller disturbances, the transition starts at about the same point and its vorticity flows downstream.

ACKNOWLEDGEMENTS

The authors wish to express their thanks to Dr. Y. Oshima and Mr. Y. Ishii for their full cooperation with the experiments and to Mr. Jacob E. Fromm for helpful discussions.

REFERENCES

[1] Arakawa, M. and Matsunobu, Y.: Proceedings of the 16th Symposium on Turbulence, Japan Society of Fluid Mechanics, 1984.
[2] Arakawa, M. and Matsunobu, Y.: Proceedings of the 17th Symposium on Turbulence, Japan Society of Fluid Mechanics, 1985.
[3] Davey, A. and Grazin, P. G.: The stability of Poiseuille flow. JEM **36**, 209–218 (1969).
[4] Dixon, T. N. and Hellums J. D.: A study on stability and incipient turbulence in Poiseuille and plane-Poiseuille flow by numerical finite-difference simulation, A.I.Ch.E. J. **13**, 866–872 (1967).
[5] Garg, V. K. and Rouleau, W. T.: Linear spatial stability of pipe Poiseuille flow. JFM **54**, 113–127 (1972).
[6] Gill, A. E.: On the behaviour of small disturbances to Poiseuille flow in a circular pipe. JFM **21**, 145–172 (1965).
[7] Goldstein, S.: Modern developments in fluid dynamics, Dover publications, 1965.
[8] Huang, L. M. and Chen, T. S.: Stability of developing pipe flow subjected to non-axisymmetric disturbances. JFM **63**, 183–193 (1974).
[9] Huang, L. M. and Chen, T. S.: Stability of the developing laminar pipe flow. Phys. Fluids **17**, 245–247 (1974).
[10] Kanda, H., Oshima, K.: Proceedings of the Symposium on Mechanics for Space Flight-SP **4**, 1986.
[11] Kanda, H., Oshima, K.: Proceedings of the 10th International Conference on Numerical methods in Fluid Dynamics, 1986.
[12] Kanda, H., Oshima, K. and Ishii, Y.: Proceedings of the Japan Society for Aeronautical and Space sciences, 1986.
[13] Kawamura, T.: Proceedings of the 17th Symposium on Turbulence, Japan Society of Fluid Mechanics, 140–144 (1985).
[14] Koyari, Y.: Study of Unsteady Entrance Flow in Pipes, PhD Thesis, Tokyo University, 1980.
[15] Kuwabara, S.: Nonlinear stability of the plane Couette and the Hagen-Poiseuille flows. J. Phys. Sloc. Jpn. **33**, 828–837 (1972).
[16] Kyrazis, D. T.: A Numerical Modeling of the Fluid Dynamic Stability of Hagen-Poiseuille Flow, PhD Thesis, University of California/Livermore (UCRL-52289), 1977.
[17] Langhaar, H. L.: Steady Flow in the Transition Length of a Straight Tube, J. Appl. Mechanics, **9**, A55–A58 (1942).
[18] Leite, R. I.: An experimental investigation of the stability of Poiseuille flow, JFM **5**, 81–96 (1959).
[19] Lin, C. C.: On the stability of two-dimensional parallel flows, Quart. Appl. Math. **3**, 117, 218, 277 (1945–1946).
[20] Mohanty, A. K. and Asthana, S.B.L.: Laminar flow in the entrance region of a smooth pipe, J. Fluid Mech., **90**433–447 (1978).
[21] Prandtl, L. and Tietjens, O. G.: Applied Hydro- and Aeromechanics, Dover Publications, 1934.
[22] Ramaprian, B. R. and Tu, S. W.: An experimental study of oscillatory pipe flow at transtional

Reynolds numbers. JFM **100**, 513–544 (1980).

[23] Reynolds, O.: An Experimental Investigation of the Circumstances which determine whether the Motion of Water shall be Direct or Sinuous, and of the Law of Resistance in Parallel Channels. Trans. Roy. Soc. London **174**, 935–982 (1883).

[24] Salwen, H. and Grosch C. E.: The stability of Poiseuille flow in a pipe of circular cross-section. JFM **54**, 93–112 (1972).

[25] Schiller, L.: Die Entwicklung der laminaren Geschwindigkeits-verteilung und ihre Bedeutung fur Zahigkeitsmessungen. ZAMM **2**, 96–106 (1922).

[26] Schlichting, H.: Boundary-Layer Theory (7th edition), McGraw-Hill, 1978.

[27] Sparrow, E. M. and Lin, S. H.: Flow development in the hydrodynamic entrance region of tubes and ducts. Phys. Fluids **7**, 338–347 (1964).

[28] Stettler, J. C. and Hussain, A.K.M.F.: On transition of the pulsatile pipe flow. JFM **170**, 169–197 (1986).

[29] Tatsumi, T.: Stability of the laminar inlet-flow prior to the formation of Poiseuille regime, 2. J. Phys. Soc. Jpn. **7**, 495–502 (1952).

[30] Vrentras, J. S., Duda, J. L. and Bargeron, K. G.: Effect of Axial Diffusion of Vorticity on Flow Development in Circular Conduits: Part 1. Numerical Solution, A.I.Ch.E.J. **12**, 837 (1966).